CHAOTIC NEOCLASSICAL TRANSPORT AT AZIMUTHALLY PERTURBED OR WAVE-MINGLED SEPARATRIX

A.A. Kabantsev, D.H.E. Dubin, Yu.A. Tsidulko[*], and C.F. Driscoll

University of California at San Diego, La Jolla, CA 92093, USA, akabantsev@ucsd.edu
[*]Budker Institute of Nuclear Physics, Novosibirsk 630090, Russia

Variations in magnetic or electrostatic confinement fields give rise to trapping separatrices, and standard neoclassical transport theory analyzes effects from collision-induced separatrix crossings. Experiments and theory have now characterized novel transport effects arising from "chaotic" separatrix crossings, which occur due to equilibrium plasma rotation across θ-ruffled separatrices, and/or due to wave-induced separatrix fluctuations.

I. INTRODUCTION

Neoclassical transport due to axial asymmetries is ubiquitous in magnetic fusion plasma confinement. These plasmas typically have several locally-trapped particle populations (either by chance, design, or due to magnetic coil discreteness), partitioned by separatrices from one another and from passing particles. The drift orbits for particles trapped in the two separate regions may be displaced radially from one another due to a global asymmetry, leading to the standard neoclassical ripple transport as particles collisionally change (at rate ν) from trapped to passing and back. Neoclassical transport theory analyzes the particle transport and wave effects arising from collisional separatrix scatterings in a variety of geometries [1-4], and experimental corroboration has been obtained in some regimes of strong collisions [5, 6].

This situation is dramatically modified when the separatrices are themselves θ-asymmetric (*ruffled*), or when they fluctuate due to waves propagating in plasmas. In such a case the drifting particles see a time-varying separatrix barrier, and without needing strong collisions they can *chaotically* transit from trapped to passing and back. This mechanism has previously been taken to be ineffective because of presumed symmetries of such transitions [7].

In our experiments these chaotic separatrix crossing lead to significantly enhanced neoclassical transport in the low collisionality regimes associated with fusion plasmas. The experiments have externally controlled ruffles or fluctuations on the separatrix, and can thus identify the novel *chaotic* neoclassical ripple transport scaling as $\nu^0 B^{-1}$ as distinct from *collisional* neoclassical ripple transport scaling as $\nu^{1/2} B^{-1/2}$.

II. EXPERIMENTAL SETUP

The pure electron plasma columns utilized here are confined in a cylindrical Penning-Malmberg trap [8-10]. Electrons are confined radially by a nominally uniform axial magnetic field $0.4 < B < 20$ kG; and are confined axially by voltages $V_c = -100$ V on end cylinders of radius $R_w = 3.5$ cm. The electron columns have length $L_p = 49$ cm, and radial density profile $n(r)$ with central density $n_0 \approx 1.6 \times 10^7 \text{cm}^{-3}$ and line density $N_L = \pi R_p^2 n_0 \approx 6.1 \times 10^7 \text{cm}^{-1}$. The unneutralized charge results in an equilibrium potential energy $\Phi_e(r)$ with $\Phi_{e0} \approx +28$ eV at $r = 0$ (here, all Φ's are in energy units). This gives an $E \times B$ drift rotation $f_E(r)$ which decreases monotonically from $f_E \approx 230\text{kHz} \times (B/1\text{kG})^{-1}$. The electrons have a near-Maxwellian velocity distribution with thermal energy $T \lesssim 1$eV, giving axial bounce frequency $f_b \approx 430$ kHz and rigidity $\mathcal{R} \equiv f_b / f_E \approx 2 B_{\text{kG}}$.
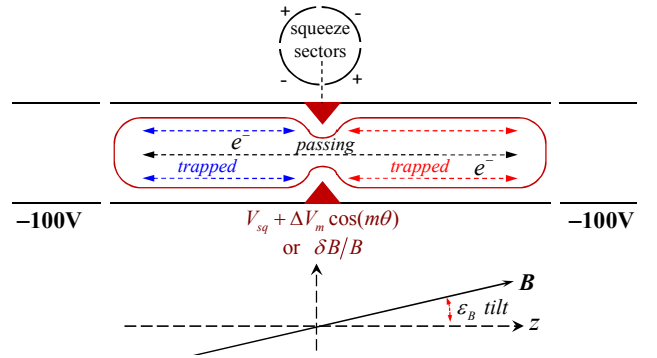
Fig. 1. Schematic of electron plasma with tilt ε_B and a trapping barrier in a cylindrical Penning-Malmberg trap.

An electrostatic trapping barrier $\phi_s(r, \theta)$ is created by a "squeeze" wall voltage V_{sq} (see Fig. 1) with adjustable θ-components $\pm \Delta V_m$. This gives interior separatrix energy $\phi_s(r, \theta) = \phi_{s0}(r) + \Delta \phi_m \cos[m(\theta - \theta_m)]$. Here we focus mostly on the $m = 2$ ruffles, created by voltages $\pm \Delta V_2$ applied to four 60° sectors, extending over $\Delta z = 3.8$ cm near the $z = 0$ center. At every radius, low energy particles are trapped in either the left or right end, whereas higher energy untrapped particles transit the entire length of the column. Ruffles spread the

characteristic separatrix energy by $\Delta\phi_m(r) \lesssim \Delta V_m (r/R_w)^m$, reduced by plasma shielding.

Particles change from trapped to untrapped (and vice versa) due to collisions, due to drift-rotation across θ-ruffles, or due to temporal fluctuations $\Delta\phi(t)$ in the separatrix energy. The electron-electron collisionality of the present experiments is relatively low ($\nu \sim 100$/sec); collisions acting for a drift-rotation period spread parallel velocities at the separatrix by an energy width $\Delta W_c \equiv T(\nu/2\pi f_E)^{1/2}(\phi_{s0}/T)^{1/2} \approx 0.02\text{eV}\times(B/1\text{kG})^{1/2}$. The *chaotic* collisionless (de)trapping processes will be important when $\Delta\phi_m(r) \geq \Delta W_c$, or when $\Delta\phi(t) \geq \Delta W_c$.

We diagnose the bulk expansion rate $\nu_{<r2>}$ defined as

$$\nu_{<r2>} \equiv \frac{1}{\langle r^2 \rangle}\frac{d\langle r^2 \rangle}{dt}. \qquad (1.1)$$

Fortunately, it can be accurately and readily obtained from the continuous frequency shift $f_2(t)$ of a small amplitude $m = 2$ diocotron mode, as $\nu_{<r2>} = (1/f_2)df_2/dt$. The bulk expansion rate $\nu_{<r2>}$ is an integral measure of the full radial flux that includes both mobility and diffusive contributions, both being proportional to the radial diffusion coefficient $D_r(r)$.

III. ASYMMETRY-INDUCED TRANSPORT

Radial particle transport is conveniently driven by a small magnetic tilt asymmetry with controlled magnitude $\varepsilon_B \equiv B_\perp/B_z \lesssim 0.001$ and gradually chosen tilt direction $\theta_B \equiv \tan^{-1}(B_y/B_x)$. The left-right asymmetric $(\overline{\delta\phi_L} \neq \overline{\delta\phi_R})$ interior potential perturbations (caused by the tilt) provide that left- and right-end trapped particles have different drift orbits, giving neoclassical radial diffusion coefficient

$$D_r(r) = \overline{f}_E\left[(\overline{\delta\phi_L} - \overline{\delta\phi_R})\big/\partial\Phi_e/\partial r\right]^2 \\ \times\tfrac{1}{4}F_M(\phi_{s0})\{\Delta W_c D_{cA} + \Delta\phi_2 D_{2A}\sin^2\alpha\}, \qquad (1.2)$$

where F_M is the Maxwellian distribution of energies. Both the collisional bounce-Averaged transport coefficient D_{cA} and the $m = 2$ ruffle coefficient D_{2A} are shown in Fig. 2, calculated as functions of the normalized ruffle strength $\Delta\phi_2/\Delta W_c$. While the ruffle-induced transport coefficient D_{2A} is nearly independent of $\Delta\phi_2/\Delta W_c$, the collisional coefficient D_{cA} shows a fast decline as collisionless particle transitions smooth out the discontinuity of F_M.

Figure 3 shows how in theory the transformation from predominantly collisional neoclassical diffusion to the chaotic regime (ruffle dominated, $\propto \Delta\phi_2 D_{2A}$) occurs. For a quick comparisons with the experiments it can be rather conveniently approximated as

$$D_* \equiv \Delta W_c D_{cA} + \Delta\phi_2 D_{2A}\sin^2\alpha \\ \approx 4(\Delta\phi_2\sin^2\alpha + 0.88\Delta W_c e^{-\frac{\Delta\phi_2}{0.88\Delta W_c}}). \qquad (1.3)$$
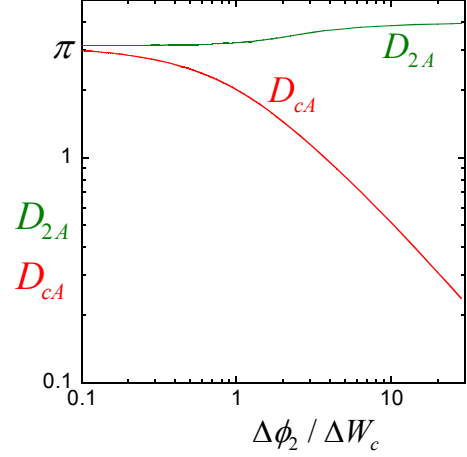
Fig. 2. Calculated collisional D_{cA} and ruffle induced D_{2A} coefficients versus the normalized ruffle strength.
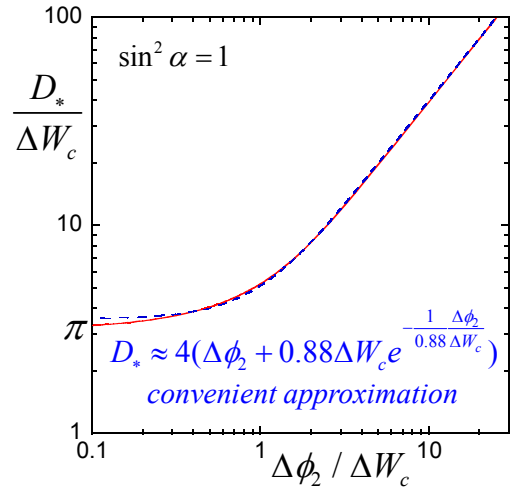
Fig. 3. Combined neoclassical transport coefficient D_* versus the normalized ruffle strength. The dashed line shows used approximation.
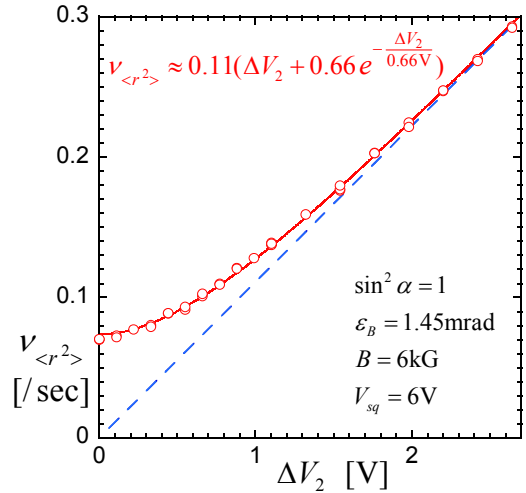
Fig. 4. Measured expansion rate as a function of the ruffle voltage ΔV_2 at the wall.

Figure 4 shows the measured expansion rate $\nu_{<r^2>}$ for the case $\sin^2\alpha = 1$ as a function of ruffle voltages $\pm\Delta V_2$ at the wall. It has essentially the same fitting function as in Fig. 3, giving the normalized "radially averaged" ruffle strength as $\langle\Delta\phi_2/\Delta W_c\rangle_r \approx (4/3)\Delta V_2/1\text{V}$, which is close to the calculated value. Thus, at $B = 6$ kG and $\Delta V_2 = 3$V the effective ruffle width $\Delta\phi_2 \approx 4\Delta W_c$, and the transport rate has changed by 4× accordingly.
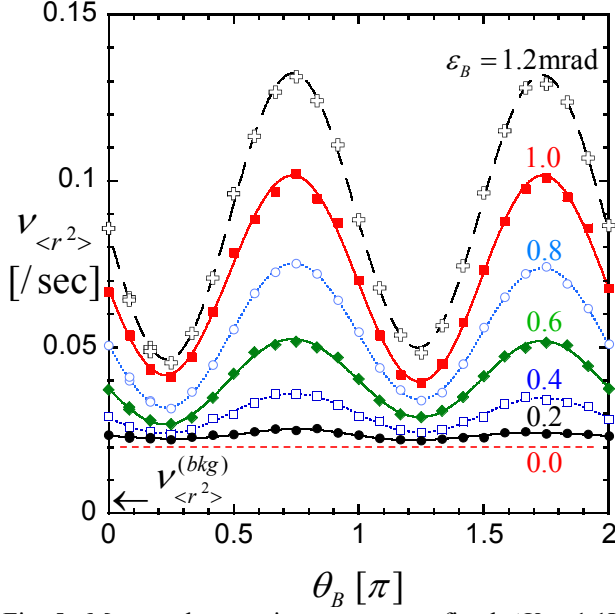
Fig. 5. Measured expansion rate $\nu_{<r^2>}$ at fixed $\Delta V_2 = 1.1$V showing chaotic part of neoclassical transport varying as $\varepsilon_B^2\sin^2\alpha$, and α-independent collisional transport.
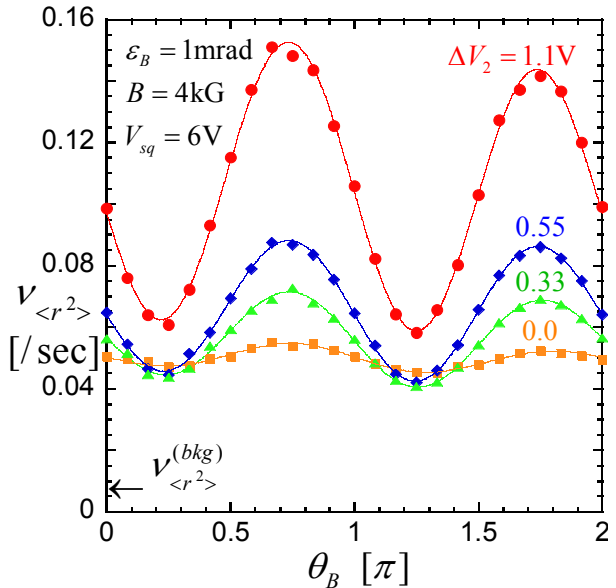
Fig. 6. Measured expansion rate $\nu_{<r^2>}$ at fixed $\varepsilon_B = 0.001$, showing chaotic part of neoclassical transport varying as $\Delta V_2 \sin^2\alpha$, and α-independent collisional transport.

Figure 5 is a plot of measured expansion rate $\nu_{<r^2>}$, taken during step-by-step rotation of the magnetic tilt orientation angle θ_B, for various tilt strengths ε_B at the fixed wall ruffle $\Delta V_2 = 1.1$V. The ruffled-induced part shows an unambiguous $\sin^2\alpha$ dependence on relative angle $\alpha \equiv \theta_B - \theta_2$, with magnitude proportional to ε_B^2; and varying θ_2 in steps of $\pi/2$ (not shown) verifies the dependence on relative angle only.

Figure 6 is a plot of measured expansion rate $\nu_{<r^2>}$ versus magnetic tilt orientation angle θ_B, for various applied wall ruffle strengths ΔV_2, now at the fixed tilt strength $\varepsilon_B = 0.001$. Once again, the ruffled-induced part shows unambiguous $\sin^2\alpha$ signature, but now with magnitude proportional to ΔV_2.

The distinctive $\varepsilon_B^2\sin^2\alpha$ signature, together with separate control of ΔV_2 and ε_B, enables experimental identification of the transport processes as

$$\nu_{<r^2>} = C_{cA}(\Delta V_2)\varepsilon_B^2 + C_{2A}\varepsilon_B^2\Delta V_2\sin^2\alpha$$
$$+ C_{cK1}\varepsilon_B^2 + C_{cK2}\Delta V_2^2 + \nu_{<r^2>}^{(bkg)}, \qquad (1.4)$$

where C_{cA} and C_{2A} represent the radial integrals of Eqn. (1.2); C_{cK1} and C_{cK2} represent collisional Kinetic (bounce-resonant) transport driven by ε_B^2 and ΔV_2^2 as z−dependent "error" fields[11,12]; and small $\nu_{<r^2>}^{(bkg)}$ arises from uncontrolled background tilts, separatrices, and omnipresent ruffles. Here, for dimensional simplicity, $\varepsilon_B \equiv \varepsilon_B/(1\text{mRad})$ and $\Delta V_2 \equiv \Delta V_2/(1\text{Volt})$.
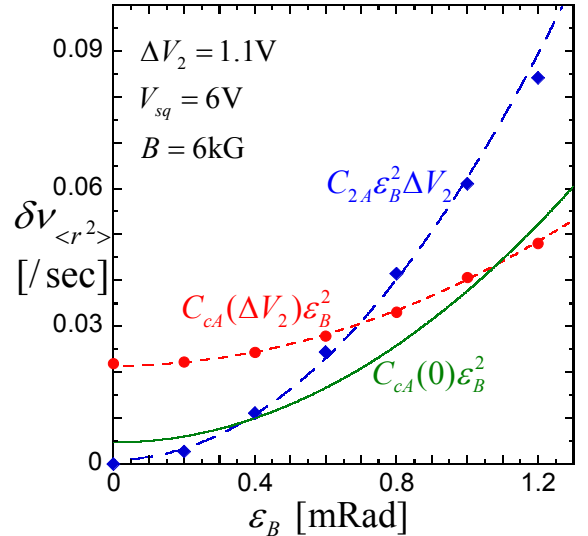
Fig. 7. Measured ε_B^2 scalings for the C_{2A} and $C_{cA}(\Delta V_2)$ neoclassical transport terms at $B = 6$kG. Every marker here (not shown for $C_{cA}(0)$) is the result of $(a + b\sin^2\alpha)$ fit as in Fig. 5.

C_{2A} and $C_{cA}(\Delta V_2)$ are readily obtained from the $\sin^2\alpha$ dependences as those shown in Figs. 5 and 6, and varying ε_B gives the expected ε_B^2 scaling, as the one shown in

Fig. 7 for $\Delta V_2 = 1.1$V and $B = 6$kG ($C_{2A} \approx 0.056$/sec). Data taken with $\Delta V_2 = 0$ define $C_{cA}(0) \approx 0.033$/sec, and just by comparing it to $C_{cA}(1.1$V$) \approx 0.019$/sec and using the $D_{cA}(\Delta\phi_2/\Delta W_c)$ data from Fig. 2, one can get another estimate on the "radially averaged" ruffle strength as $\langle\Delta\phi_2/\Delta W_c\rangle_r \approx (4/3)\Delta V_2/1$V, which is consistent with the previous conclusion based on the results shown in Figs. 3 and 4.

Data taken with $\varepsilon_B = 0$ show a $\nu_{<r2>}^{(bkg)}$ offset and a parabolic dependence on a varied ΔV_2, giving C_{cK2}. Varying ε_B then selects C_{cA} and C_{cK1}; these terms are distinguished by their B-scaling (discussed next), and by the fact that the z-antisymmetric bounce-averages in C_{cA} require the separatrix, whereas the kinetic C_{cK1} depends only weakly on the applied squeeze voltage. In Fig. 6, $C_{cK2}(4$kG$) \approx 0.03$, giving elevated $\sin^2\alpha$ minima for large ΔV_2; the depressed minima for $\Delta V_2 = 0.33$ are from ruffle-suppression of D_{cA} (see Fig. 2); and $\nu_{<r2>}^{(bkg)} \approx 0.007$/sec.
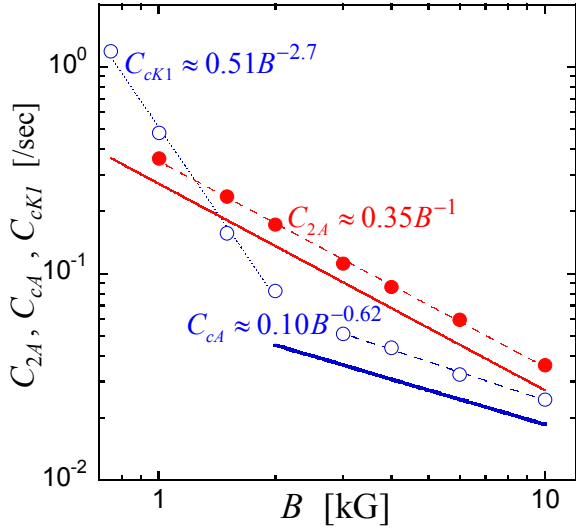
Fig. 8. Measured transport rates C_i versus B at $V_{sq} = 6$V, with empirical scalings. Solid lines are theory predictions.

Figure 8 shows the measured transport rates C_{2A}, C_{cA} and C_{cK1} versus magnetic field with empirical scalings (dashed), compared to theory (lines). At high B, the chaotic and collisional separatrix transport processes agree closely with theory, scaling as B^{-1} and $B^{-1/2}$ respectively. Here the accuracy of comparison is limited by temperature uncertainty, sensitivity to edge density gradients, and induced modification of $F_M(\phi_{s0})$. At low B, the kinetic transport labeled C_{cK1} is observed to depend strongly on field ($\propto B^{-2.7}$), but no simple power law is expected theoretically as bounce-rotation resonances become dominant. Prior scaling experiments have been confused by the presence of uncontrolled separatrices and ruffles, and by overlapping transport regimes[8].

III. CONCLUSIONS

Most plasma confinement devices have trapping separatrices, arising from variations in magnetic field strength or external potentials. These separatrices are never perfectly symmetric, or perfectly aligned with other asymmetries. If the separatrix itself is asymmetric or temporally perturbed, the drifting particles collisionlessly change from trapped to passing and back, leading in the case of low collisionality to enhanced transport ($\propto \nu^0 B^{-1}$) in comparison to the standard neoclassical ripple transport ($\propto \nu^{1/2}B^{-1/2}$). When the separatrix layer collisional width becomes less than its (symmetry) perturbations, this new loss mechanism is the dominant bulk transport process in our non-neutral plasma experiments, and it could have important implications for similar low collisionality regimes in other magnetic conferment experiments.

REFERENCES

1. P. HELANDER and D.J. SIGMAR, *Collisional Transport in Magnetized Plasmas*, Cambridge Monographs on Plasma Physics, Cambridge Univ. Press (2002).
2. M.N. ROSENBLUTH, D.W. ROSS and D.P. KOSTOMAROV, *Nucl. Fusion*, **12**, 3 (1972).
3. T.J. HILSABECK and T.M. O'NEIL, *Phys. Plasmas*, **10**, 3492 (2003).
4. D.H.E. DUBIN, *Phys. Plasmas*, **15**, 072112 (2008).
5. T. Ohkawa, J.R. Gilleland, and T. TAMANO, *Phys. Rev. Lett.*, **28**, 1107 (1972).
6. M.C. ZarnstoRFF, K. McGuire, M.G. Bell, B. Grek, D. Johnson, D. McCune, H. Park, A. RAMSEY, and G. TAYLOR, *Phys. Fluids B*, **2**, 1852 (1990).
7. H. MYNICK, *Phys. Fluids*, **26**, 2609 (1983).
8. A.A. Kabantsev and C.F. Driscoll, *Phys. Rev. Lett.*, **89**, 245001 (2002).
9. A.A. Kabantsev, T.M. O'Neil, Y.A. Tsidulko and C.F. Driscoll, *Phys. Rev. Lett.*, **101**, 065002 (2008).
10. A.A. KABANTSEV and C.F. DRISCOLL, *Phys. Rev. Lett.*, **97**, 095001 (2006).
11. D.L. EGGLESTON and T.M. O'NEIL, *Phys. Plas.*, **6**, 2699 (1999); D.L. EGGLESTON and J.M. WILLIAMS, *Phys. Plas.*, **15**, 032305 (2008).
12. E.P. GILSON and J. FAJANS, *Phys. Rev. Lett.*, **90**, 015001 (2003).